

Future changes in Beijing haze events under different anthropogenic aerosol emission scenarios

Lixia Zhang^{1,2}, Laura J. Wilcox³, Nick J. Dunstone⁴, David J. Paynter⁵, Shuai Hu^{1,6},
Massimo Bollasina⁷, Donghuan Li⁹, Jonathan K. P. Shonk^{3,8}, and Liwei Zou¹
1 LASG, Institute of Atmospheric Physics, Chinese Academy of Sciences, Beijing, China
2 Collaborative Innovation Center on Forecast and Evaluation of Meteorological
Disasters, Nanjing University of Information Science & Technology, Nanjing, 210044,
China
3 National Centre for Atmospheric Science, Department of Meteorology, University of
Reading, UK
4 Met Office Hadley Centre, FitzRoy Road, Exeter EX1 3PB, UK
5 NOAA/Geophysical Fluid Dynamics Laboratory, Princeton, New Jersey
6 University of Chinese Academy of Sciences, Beijing 100049, China
7 School of Geosciences, Grant Institute, University of Edinburgh, Edinburgh, UK
8 Now at: MetOffice@Reading, Department of Meteorology, University of Reading,
UK
9 Key Laboratory of Water Cycle and Related Land Surface Processes, Institute of
Geographic Sciences and Natural Resources Research, Chinese Academy of Sciences

Submitted to Atmospheric Chemistry and Physics

Revised on 17th Jan, 2021

Corresponding author: Dr. Lixia Zhang

LASG, Institute of Atmospheric Physics, Chinese Academy of Sciences, Beijing
100029, China

Phone: 86-10-8299-5456

Email: lixiazhang@mail.iap.ac.cn

28 **Abstract:** Air pollution is a major issue in China and one of the largest threats to public
29 health. We investigated future changes in atmospheric circulation patterns associated
30 with haze events in the Beijing region, and the severity of haze events during these
31 circulation conditions, from 2015 to 2049, under two different aerosol scenarios: a
32 maximum technically feasible aerosol reduction (MTFR) and a current legislation
33 aerosol scenario (CLE). In both cases greenhouse gas emissions follow the
34 Representative Concentration Pathway (RCP) 4.5. Under RCP4.5 with CLE aerosol the
35 frequency of circulation patterns associated with haze events increases due to a
36 weakening of the East Asian winter monsoon via increased sea level pressure over the
37 North Pacific. The rapid reduction in anthropogenic aerosol and precursor emissions in
38 MTFR further increases the frequency of circulation patterns associated with haze
39 events, due to further increases of the sea level pressure over the North Pacific and a
40 reduction in the intensity of the Siberian high. Even with the aggressive aerosol
41 reductions in MTFR periods of poor visibility, represented by above normal aerosol
42 optical depth (AOD), still occur in conjunction with haze-favorable atmospheric
43 circulation. However, the winter mean intensity of poor visibility decreases in MTFR,
44 so that haze events are less dangerous in this scenario by 2050 compared to CLE, and
45 relative to the current baseline. This study reveals the competing effects of aerosol
46 emission reductions on future haze events through their direct contribution to pollutant
47 source and their influence on the atmospheric circulation. A compound consideration
48 of these two impacts should be taken in future policy making.

49 **Key Words:** air-pollution, anthropogenic aerosol, atmospheric circulation, haze events

50

Deleted: 6

Deleted: 50

1. Introduction

The increases in aerosol and precursor emissions in China due to the rapid economic development and urbanization in recent decades have caused more frequent and severe haze events. Beijing and the surrounding area is the most polluted region in China (Niu et al., 2010; Ding and Liu, 2014; An et al., 2019; Chen and Wang, 2015). Air pollution has become one of the major issues in China, and the greatest threat to public health. Since the implementation of the “Atmospheric Pollution Prevention and Control Action Plan” in 2013 (China State Council, 2013), aerosol emissions have dramatically decreased, with sulfur dioxide (SO₂) reduced by 59% in 2017 compared to 2013 (Zheng et al., 2018). However, haze events have still occurred regularly in recent years, as, in addition to being influenced by aerosol emissions, meteorological conditions, including limited scavenging, dispersion and ventilation, have been found to play important roles in the variation of air-quality in northern China (An et al., 2019; Pei et al., 2018; Cai et al., 2017). Such events are typically associated with the occurrence of large-scale atmospheric circulation patterns favoring the accumulation of pollutants (Chen and Wang, 2015; Zhang et al., 2014). Locally, a strong temperature inversion in the lower troposphere, weak surface winds, and subsiding air in the planetary boundary layer are favorable for the development and persistence of haze events (Wu et al., 2017; Feng et al., 2018). As anthropogenic aerosol has the potential to induce changes in the atmospheric circulation, in addition to making a direct contribution to the chemical composition of haze, it is crucial to understand how changes in aerosol emissions might

74 contribute to the frequency and intensity of haze events in future.

75 On interannual time scales, the East Asian winter monsoon (EAWM) is significantly
76 negatively correlated with aerosol concentrations in Beijing, due to the associated high
77 frequency of extreme anomalous southerly episodes in North China, a weakened East
78 Asian trough in the mid-troposphere and a northward shift of the East Asian jet stream
79 in the upper troposphere (Jeong and Park, 2017; Li et al., 2016; Pei et al., 2018). The
80 cold air process over Beijing is favorable for pollutant dispersion and transport outside
81 because of the accompanied large near-surface wind speed and deep mixing layer. A
82 low occurrence of cold air processes in the recent winters of 2013, 2014 and 2017 has
83 resulted in severe pollution (He et al., 2018). In the past decades, the weakening of the
84 EAWM was found to contribute to the increased frequency of haze events over North
85 China (Chen and Wang, 2015; An et al., 2019). Arctic sea ice extent also has been
86 linked to increased stability over eastern China, explaining 45%~67% of the interannual
87 to interdecadal variability of winter haze days over eastern China (Wang et al., 2015).
88 Overall, around half of the variability in the frequency of haze events in Beijing is
89 controlled by meteorological conditions, while both meteorological conditions and
90 aerosol emissions contribute to the intensity (Pei et al., 2020). Internal climate
91 variability has contributed to the rapid increase of early winter haze days in North China
92 since 2010 (Zhang et al., 2020).

93 Anthropogenic forcing, estimated by using large ensemble runs with and without
94 anthropogenic forcings, has also increased the probability of the atmospheric patterns

95 conducive to severe haze in Beijing by weakening the EAWM (Li et al., 2018).
96 Projections based on Coupled Model Intercomparison Project Phase 5 (CMIP5) models
97 showed that weather conditions conducive to haze events in Beijing or eastern China
98 will increase with global warming (Horton et al., 2012, 2014), due to an increased
99 occurrence of stagnation days in response to both accelerated Arctic ice melting (Cai et
100 al., 2017; Liu et al., 2019a) and a continued weakening of EAWM (Pei and Yan, 2018;
101 Liu et al., 2019a). If there is no change in aerosol emission in future, increased
102 stagnation days and decreased light precipitation days associated with global warming
103 would also cause an increase in air pollution days in eastern China (Chen et al., 2019).
104 Regional climate model simulations under the RCP4.5 scenario showed that the air
105 environment carrying capacity, a combined metric measuring the capacity of the
106 atmosphere to transport and dilute pollutants, tends to decrease in the 21st century across
107 China (Han et al., 2017). However, there is a large uncertainty in future aerosol
108 emission pathways, with uncertainty around the sign of the change in global emission
109 rate, as well as choice of haze index, and internal climate variability (Scannell et al.,
110 2019; Callahan et al., 2019; Callahan and Mankin, 2020). Furthermore, changes in
111 aerosol emission may influence the haze-favorable atmospheric circulation, in addition
112 to their role in haze composition.

113 The interplay between the role of aerosol as a constituent of haze, and as a potential
114 driver of changes in the circulation patterns conducive to haze, have yet to be explored.
115 If the rapid reductions in aerosol and precursor emissions currently underway in China

Deleted:

Deleted: Hori et al., 2006;

continue in future, understanding the balance between the different influences of anthropogenic aerosol forcing on haze events is a key question. Typically, anthropogenic aerosol (AA) and greenhouse gases (GHGs) both vary in the future (e.g. those following the RCPs or Shared Socioeconomic Pathways), which can make their relative contributions difficult to determine. In this work, we examine future scenarios with the same GHGs emission pathway but different aerosol pathways in order to separate the role of AA forcing. We address the following two questions: 1) Do the atmospheric conditions conducive to haze events change differently under different AA scenarios? 2) If so, how AA forcing modulate the frequency of haze-favorable circulation and the severity of the haze events change?

The remainder of the paper is organized as follows: we briefly introduce the experiment design and methods in Section 2, and show the atmospheric circulation patterns conducive to Beijing haze events in Section 3. Projected Beijing haze events under two different aerosol emissions and the underlying mechanism of projected circulation changes will be given in Section 4. We will finally provide the summary and discussion in Section 5.

2. Experiments and methods

2.1 Data and experiment design

We use observed daily visibility, relative humidity and wind speed from 1974 to 2013 from the National Climatic Data Center (NCDC) Global Surface Summary of the Day

138 (GSOD) database (Fig.S1a). Haze days are defined as days with daily visibility less
139 than 10km, relative humidity less than 90% and surface wind speed less than 7 m s^{-1}
140 (Chen and Wang, 2015). The observed haze occurrence is the number of haze days, and
141 observed haze intensity is defined as the minimum 3-day consecutive visibility
142 (VN3day). Spatial distributions of winter mean haze occurrence and VN3day are shown
143 in Fig.S1b-c. Data from the Japanese 55-year Reanalysis (JRA55; Kobayashi et al.,
144 2015) dataset for the period 1958-2013 are used in this study to evaluate the model
145 representations of the present-day climate. The variations of haze index derived from
146 JRA-55 are highly consistent with those from NCEP-NCAR reanalysis (not shown).
147 We only use JRA-55 in this study.

148 Simulations with the Met Office Unified Model (Global Coupled configuration 2)
149 HadGEM3-GC2 (Williams et al., 2015) and the NOAA Geophysical Fluid Dynamics
150 Laboratory (GFDL) Climate Model version 3 (GFDL-CM3, Donner et al., 2011;
151 Griffies et al., 2011) are used to investigate the impact of different aerosol forcing
152 scenarios. HadGEM3-GC2 is run with a horizontal resolution of N216 (~60 km) in the
153 atmosphere, and $1/4^\circ$ in the ocean. GFDL-CM3 has a horizontal resolution of ~200 km
154 in the atmosphere and 1° in the ocean. Both models include a representation of aerosol-
155 cloud interactions (Ming et al., 2006; Bellouin et al., 2011).

156 Three sets of experiments were carried out with each model (Table S1): a historical
157 experiment from 1965 to 2014 and two experiments for the future (2015-2050). In the
158 historical experiment, greenhouse gases and anthropogenic aerosol and precursor

Deleted: 6

160 emissions are taken from CMIP5 (Lamarque et al., 2010; Taylor et al., 2012). The future
161 experiments have common GHG emissions following the RCP4.5 scenario, but
162 different aerosol emission pathways. The aerosol pathways are the current legislation
163 emissions (CLE) and the maximum technically feasible reduction (MTFR) taken from
164 the ECLIPSE V5a global emission dataset (Amann et al., 2015,
165 <https://iiasa.ac.at/web/home/research/researchPrograms/air/ECLIPSEv5a.html>). In
166 CLE, anthropogenic aerosol emissions are assumed to evolve following the current
167 legislation, resulting in a moderate global increase by 2050. In contrast, MTFR assumes
168 a full implementation of the most advanced technology presently available to reduce
169 aerosol emissions by 2030, which results in their rapid global decrease over this period.
170 The regional changes in AA for His, CLE and MTFR can be found in Scannell et al.
171 (2019) and Luo et al. (2020).

172 We use 1984-2013 as a baseline (His), 2015-2049 as the future period, and display
173 anomalies between the two. Compared with His, CLE shows a dramatic increase in SO₂
174 over Asia, with peak values over India (not shown) and eastern China (Fig.S2a). MTFR
175 has similar changes over Europe to CLE, negligible changes over India (not shown),
176 and a dipole over China, with a weak increase to the north and a decrease to the south
177 (Fig.S2b). Thus, a dramatic decrease in SO₂ in MTFR relative to CLE is seen over the
178 whole Asian continent, particularly over the Beijing region (Fig. S2c).

179 2.2 Haze weather index and East Asian winter monsoon index

Deleted: 0
Deleted: 0
Deleted: 4
Deleted: 6
Deleted: 50

185 We focus on haze events during the winter (December-February) around Beijing where
186 Chinese haze events are most frequent and severe (Niu et al., 2010; Chen and Wang,
187 2015). In this study, we use the haze weather index (HWI) proposed by Cai et al. (2017)
188 as it has also been shown to have a strong relationship with PM_{2.5} concentrations in
189 Beijing.

190 The HWI comprises three constituent terms representing the vertical temperature
191 gradient in the troposphere (ΔT), the 850-hPa meridional wind (V850), and the north—
192 south shear in the 500-hPa zonal wind (U500) (see boxes and lines in Fig.1). ΔT is
193 calculated as the difference between the 850 hPa temperature averaged over (32.5°–
194 45°N, 112.5°–132.5°E) and the 250-hPa temperature averaged over (37.5°–45°N,
195 122.5°–137.5°E). V850 is the 850hPa meridional wind averaged over the broader
196 Beijing region (30°–47.5°N, 115°–130°E), and U500 is a latitudinal difference between
197 the 500-hPa zonal wind averaged over a region to the north of Beijing (42.5°–52.5° N,
198 110°–137.5°E) and a region to the south (27.5°–37.5°N, 110°–137.5°E). Each of the
199 three terms is normalized by their standard deviation over the reference period (here
200 1984–2013). The three variables are added together to create the HWI, which is then
201 normalized again by its standard deviation over the reference period. A positive HWI
202 represents conditions that are unfavorable to air-pollutant dispersion, and days with
203 HWI>0 are regarded as “haze events”. The HWI defined by Cai et al. (2017) made use
204 of daily data. Due to unavailability of model data at daily resolution, we instead used

Deleted: 0

Deleted: 04

207 monthly data. The reliability of using HWI calculated from monthly mean variables
208 will be discussed in Section 3 based on reanalysis.

209 The strength of the EAWM is quantified using the index defined by Wang and Chen
210 (2014). This index takes into account both the east-west and the north-south pressure
211 gradients and is defined as:

$$212 \quad \text{EAWM} = (2 \times \text{SLP}_1 - \text{SLP}_2 - \text{SLP}_3) / 2$$

213 Where SLP_1 , SLP_2 and SLP_3 represent normalized sea level pressure (SLP) averaged
214 over Siberia (40-60°N, 70-120°E), the North Pacific (30-50°N, 140°E-170°W) and the
215 Maritime Continent (20°S-10°N, 110-160°E), respectively (see the boxes in Fig.S3).

216 The three components are converted to anomalies and normalized by their standard
217 deviation over the reference period (here 1984-2013). As the EAWM is directly linked
218 to the occurrence of favorable conditions for haze in Beijing (Pei et al., 2018; Liu et al.,
219 2019b; Hori et al., 2006), we therefore use this index as an additional metric to assess
220 the potential changes in future haze events under the CLE and MTR scenarios, and
221 confirm the robustness of the changes indicated by HWI.

222 2.3 Significance test

223 To test whether projected winter mean HWI change and frequency of month with
224 $\text{HWI} \geq 1$ are statistically significant, we estimated internal variability by performing a
225 Monte Carlo approach (Zhang and Delworth, 2018). We first randomly select a 90-
226 month (to mimic the DJF months for 1984-2013) period from all simulations of baseline.

Deleted: 0

Deleted: 04

Deleted: bootstrapped samples

Deleted: This resampling-based procedure involves three steps.

Deleted: First, w

Deleted: 75

234 and calculate the time-mean of HWI and frequency of months with $\text{HWI} \geq 1$ of this
 235 sample. Then, we calculate the differences between this sample and the baseline. This
 236 difference results only from internal climate variability. We repeat the first step 5000
 237 times, and the 5000 bootstrapped samples can be viewed as internal variability of
 238 baseline. For the future projections, we did the similar calculation as the baseline, but
 239 by randomly selecting a 105-month period (to mimic DJF months for 2015-2049) from
 240 projection and calculate its difference with the baseline. We then compare the medium
 241 anomalies of future projection with the ranges of the bootstrapped samples. When the
 242 median from future projection falls outside the interquartile range of baseline, we then
 243 claim that the projected changes are statistically significant (Wilconx et al., 2020). We

244 also employed a two-sample Kolmogorov-Smirnov test to determine if the probability
 245 density function (PDF) distributions are significantly different (Chakravarti et al., 1967).

246 3. Favorable climatic conditions for Beijing haze events in reanalysis

247 The circulation anomalies averaged over the days with daily $\text{HWI} > 0$ are shown in
 248 Fig.1a, c, e. The vertical temperature profile shows warmer air at the lower to mid-
 249 levels, centered around 850hPa and cold anomalies aloft 250hPa (Fig.1a). Thus, the
 250 atmosphere is stable, unfavorable for the vertical dispersion of pollutants. At the mid-
 251 latitude (500hPa), we see northward shifted mid-level westerly jets (Fig.1c). The
 252 weakened westerly winds along 30°N inhibit the horizontal dispersion of pollutants in
 253 Beijing. At the lower-level, the anomalous southerly winds at 850hPa along the East
 254 Asian coast lead to a reduction in the prevailing surface cold northerlies in winter

Deleted: (135-month), i.e. 25-yr (45-yr) winters, from His (projections),

Deleted: change of the 75-month relative to His or

Deleted: e

Deleted: 75-month

Deleted: The 75-month and 135-month are selected to mimic any 25-yr in the period 1980-2004 and 45-yr in 2016–2050, respectively; We

Deleted: 2000

Deleted: 2000

Deleted: His or future projections

Deleted: We then compare the results of model ensemble mean with the 2000 bootstrapped samples. If it falls outside the top 5% of the distribution, we then claim that the projected changes in mean HWI or frequency of month with $\text{HWI} \geq 1$ are statistically significant at the 5% level and beyond the variability of internal variability.

272 (Fig.1e). This reduction favors warmer conditions at lower levels and increased
273 moisture over Beijing, thus increasing the likelihood of haze formation and
274 maintenance.

275 The HWI was defined based on daily data. Due to limitations in data availability, we
276 instead used monthly data to calculate HWI. To determine the reliability of this
277 approach, we first examined the relationship between the magnitude of HWI calculated
278 from monthly data (HWI-month) and the number of days with daily HWI (HWI-daily) >
279 0 in the JRA-55 reanalysis during the period 1958-2013 (Fig. 2a-b). The variability of
280 HWI-month is highly consistent with that of number of days with HWI-daily>0 ($r =$
281 0.97). When HWI-month is greater than 0, about 50% days in that month are recognized
282 with HWI-daily>0, and up to 62% days with HWI-daily >0 when HWI-month ≥ 1 . In
283 this study, we define favorable climatic conditions of haze events around Beijing as a
284 month where HWI-month ≥ 1 .

285 We also checked the observed winter haze occurrence and intensity (VN3day)
286 anomalies when HWI-month ≥ 1 . More haze occurrence and reduced visibility are
287 observed over North China, indicating the reliability of using HWI-month ≥ 1 as a proxy
288 of the favorable climatic conditions for the haze events in Beijing and the surrounding
289 region. The selection of a higher threshold of HWI-month (e.g. 1.5) does not make a
290 great difference to our results (not shown). The circulation anomalies averaged over
291 HWI-month ≥ 1 (Fig. 1b, d, f) and HWI-daily > 0 (Fig. 1a, c, e) are also consistent with
292 each other, except that the anomalies for HWI-month ≥ 1 are weaker, as would be

293 expected. The spatial and temporal consistency of HWI anomalies calculated from
294 monthly and daily data confirms the suitability of our use of monthly data to explore
295 changes in the frequency of Beijing haze events associated circulation. In the following
296 sections, we will use the term HWI to indicate HWI-month for brevity.

297 **4. Changes in Beijing haze events under two AA emission scenarios**

298 *4.1 Changes in the frequency of haze-favorable circulation patterns*

299 Both HadGEM3-GC2 and GFDL-CM3 well simulate the key spatial features of the
300 large-scale atmospheric circulation in winter, when compared to JRA-55 for 1980-2004
301 (Fig.S4). Key features include the westerly jet along 30°N, the East Asian trough, and
302 northerly winds along the East Asian coast, which are caused by the zonal thermal
303 contrast and subsequent pressure gradient between the North Pacific and the Eurasian
304 continent. The models can also reliably capture the vertical temperature difference, the
305 weaker East Asian trough and the anomalous 850-hPa southerly winds associated with
306 haze events (Fig.S5 and Fig.1). The good performance of HadGEM3-GC2 and GFDL-
307 CM3 in simulating the winter monsoon and haze-favorable circulation justifies the use
308 of these two models to estimate HWI changes.

309 There is a large interannual variability in HWI, and no significant trend in HWI either
310 in His, CLE or MTFR (not shown). However, the two models both show an increase in
311 the mean HWI with no consistent change in the standard deviation (Fig.3a, c). The
312 mean HWI in His (1984-2013), CLE (2015-2049) and MTFR (2015-2049) is 0.00, 0.26,

Deleted: 0
Deleted: 04
Deleted: 6
Deleted: 50
Deleted: 6
Deleted: 50
Deleted: 39

320 and 0.50 in HadGEM3-GC2. In GFDL-CM3 it is 0, 0.32, and 0.41. There is a slight
 321 increase in the standard deviation of HWI in HadGEM3-GC2 from His (1.0) and CLE
 322 (1.0) to MTFR (1.06), while no change is seen in GFDL-CM3. The occurrence of
 323 positive HWI in CLE and MTFR increases relative to His in both models. In both
 324 models, the PDF distributions of HWI in His and CLE are significantly different at the
 325 1% level using a Kolmogorov-Smirnov test. For the distributions of HWI in CLE and
 326 MTFR, they are also significantly different at the 1% level in HadGEM3-GC2, but not
 327 in GFDL-CM3. The changes in the frequency of different HWI can be found from the
 328 cumulative distribution function (CDF) of HWI (Fig.3b, d). The frequency of $HWI \geq 1$
 329 for His, CLE and MTFR is ~16% (16%), 22% (25%), and 30% (29%) in HadGEM3-
 330 GC2 (GFDL-CM3), respectively. If AA emissions follow the CLE scenario, the
 331 frequency of month with $HWI \geq 1$ will increase by 6% and 9% in HadGEM3-GC2 and
 332 GFDL-CM3, respectively. The rapid reduction in AA emissions in MTFR contributes
 333 to an extra 4~8% increase in HWI relative to CLE in both models.

334 We used a Monte Carlos approach to test whether the changes in winter mean HWI and
 335 frequency of months with $HWI \geq 1$ among His, CLE and MTFR are significantly
 336 different from each other (Fig.4). The time-mean HWI and frequency ($HWI \geq 1$) in CLE
 337 and MTFR are both statistically different from that in His in the two models. We also
 338 see samples in CLE and MTFR change beyond the range of His in both models,
 339 although only in HadGEM3-GC2 simulations is the time-mean HWI in MTFR
 340 statistically significant from that in CLE (Fig. 4a). An examination of the future changes

Deleted: 65

Deleted: 46

Deleted: 60

Deleted: 8

Deleted: 8

Deleted: 31

Deleted: 4

Deleted: 37

Deleted: 10

Deleted: 15

Deleted: 6

Deleted: bootstrapping

Deleted: mean

in each component of the HWI is shown in Fig.S6. The shift of HWI towards more positive values from His to CLE, with a larger shift in MTFR relative to His, is found in all three components except that in V850 in GFDL-CM3. The distributions of all the component terms of the His are statistically different from CLE and from MTFR at the 5% level in both models by using a two-sample Kolmogorov-Smirnov test, while the distributions in CLE and MTFR are significantly different in HadGEM3-GC2 only, consistent with our conclusion based on the Monte-Carlo approach (Figures not shown). The changes of the three components of HWI demonstrate the atmospheric conditions favoring haze events all become more likely with global warming, and that future AA reductions may further increase their likelihood.

4.2 Possible mechanism for atmospheric circulation changes

To investigate the mechanism underlying these changes in Beijing haze-favorable circulation frequency, we present the changes in the vertical temperature profile, and spatial patterns of 850-hPa and 500-hPa winds in Figs.5-7. The lower- and mid-troposphere displays an incremental warming from His to MTFR compared to the upper levels in both models. The peak warming is at 700 hPa and over 120°-130°E. Conversely, both models simulate an upper-tropospheric cooling at 250 hPa in CLE compared to His, albeit of smaller magnitude than the warming below (Fig.S7). However, the 250 hPa temperature changes between MTFR and CLE differ in the two models (Fig.5b, d and Fig.S7g-h). Thus, the increase in tropospheric stability in MTFR relative to CLE is mainly driven by low-level warming.

Deleted: winter HWI changes and to determine whether the frequency of month with $HWI \geq 1$ among His, CLE and MTFR are significantly different from each other (Fig.4). The difference in mean HWI between CLE vs His, MTFR vs His, and CLE vs MTFR, are also statistically significant at the 5% level in both models (Fig.4a-b). The frequency of month with $HWI \geq 1$ in CLE and MTFR are both statistically different from that in His in the two models, while only in HadGEM3-GC2 simulations is the frequency in MTFR statistically significant from that in CLE at the 5% level (Fig. 4c-d).

Possible mechanism

Deleted: bootstrapping approach

387 Following the CLE aerosol pathway, both HadGEM3-GC2 and GFDL-CM3 project an
388 anomalous 850-hPa cyclonic circulation over the northwestern Pacific (0-20°N, 120-
389 180°E) relative to His, and an anticyclonic anomaly to its north (20-50°N, 120-180°E)
390 (Fig.6a-b). This pattern bears some resemblance to the anomalous circulation
391 associated with a positive phase of the Arctic Oscillation, which may be due to melting
392 Arctic sea ice (Shindell et al., 1999; Fyfe et al., 1999; Wang et al., 2020). The southerly
393 wind anomalies over eastern China, on the western flank of the anomalous anticyclone,
394 act to weaken the East Asian winter monsoon and reduce its low-level winds, making
395 conditions favorable for air-pollutant transport from south to north and air-pollutant
396 accumulation more likely. With the addition of rapid AA reductions following MTFR,
397 the 850-hPa circulation anomalies are reinforced further (Fig6.c-d), especially in
398 HadGEM3-GC2, which simulates much stronger southerly wind anomalies along the
399 East Asian coast. GFDL-CM3 shows similar anomalies over the North Pacific in CLE
400 vs His and MTFR vs His, but distinct responses over China (Fig.6d), which likely
401 explains why GFDL-CM3 does not simulate the further shift in HWI seen in
402 HadGEM3-GC2 between CLE and MTFR (Fig.S6c, f). A northeasterly anomaly is seen
403 over southeast China in GFDL-CM3 in both CLE relative to His and MTFR relative to
404 CLE. However, the onshore flow over Beijing seen in CLE relative to His, which is
405 likely to be a key contributor to an increase in haze weather events, is not enhanced
406 further by the rapid aerosol reductions in MTFR (Fig. 6d).

407 At 500 hPa, a northward shift of the westerly jet stream is projected in CLE relative to

the current baseline, with significant positive zonal wind anomalies along 50°N and negative anomalies along 30°N in both models (Fig.7a-b). This shift is consistent with the increase in the meridional temperature gradient over the North Pacific (Fig.S7). Thus, the East Asian winter trough is weakened, bringing less cold and dry air to the Beijing area, and favoring the formation and maintenance of haze events. The reductions in AA emissions in MTFR relative to CLE significantly strengthen the above-mentioned circulation anomalies at 500 hPa in both models (Fig 7c,d), and further increase the frequency of positive U500 differences in the regions used to calculate the HWI, as seen in Fig.7c-d. The changes in 500-hPa zonal winds are consistent between the two models, demonstrating the robustness of the results.

The changes in the three components of HWI in CLE relative to His indicate a weakened EAWM with increased GHGs, with reductions in AA emissions further amplifying this effect and increasing the frequency of large-scale circulation conditions conducive to Beijing haze events. To explore how the EAWM circulation responds to reductions in AA emissions, we show surface temperature and sea level pressure changes in MTFR relative to CLE (Fig. 8). Reduced AA emissions generally amplify the impact of greenhouse gases, with more warming over the Arctic, the Eurasian continent and Northwestern Pacific. Thus, the Aleutian low is further weakened in MTFR. In addition, more warming over the Eurasian continent and Northwestern Pacific leads to a SLP decrease over Siberia and the northwestern Pacific, respectively. The main difference between the two models is found from the SLP changes over the

429 Eurasian continent in the mid-latitudes, where large negative SLP anomalies are
430 presented in HadGEM3-GC2 while there are no changes in GFDL-CM3. This may lead
431 to the less westward shift of the North Pacific anomalous anticyclonic circulation in
432 GFDL-CM3 in Fig.6d.

433 The changes of EAWM, using the Wang and Chen (2014) index, in His, CLE and
434 MTRF are shown in Fig.8e-f. The EAWM weakens in CLE compared to His (blue and
435 grey boxes in Fig.8e-f), mainly due to increased SLP over the North Pacific (SLP₂,
436 Fig.S8 b), with no systematic or significant changes in SLP over Siberia (SLP₁) and the
437 Maritime continent (SLP₃) (Fig.S8a, c). The rapid AA reductions in MTRF cause the
438 SLP over Siberia to decrease consistently in both models alongside a further increase
439 in SLP₂. The changes in SLP₂ (SLP₁) are statistically significant at the 5% (10%) level
440 in both models tested by performing bootstrapped samples (Fig.S8a, b). This further
441 weakens the east-west contrast, leading to a weaker EAWM in MTRF relative to CLE,
442 consistent with the differences between CLE and His and between MTRF and CLE
443 seen in the HWI. The response of SLP over the Maritime Continent (SLP₃) to AA
444 reductions differs between the two models, indicating a large uncertainty in the SLP₃
445 changes. Thus, the AA forcing reduction predominantly weakens the EAWM through
446 reducing the zonal thermal contrast.

447 **4.3 Changes in haze intensity associated with favoring circulation**

448 Occurrence of a haze event requires stagnant atmospheric conditions, and also a
449 pollution source. Although future aerosol reductions may cause further increases in the

Deleted: PDF distributions

Deleted: lines

Deleted: , c

Deleted: a, d

Deleted: and Fig.S8c, f

Deleted: not shown

frequency of atmospheric circulation patterns currently linked with haze events, such events may become less severe in the absence of large aerosol emissions. In this section, we will examine the projected changes in the intensity of Beijing haze events using the aerosol optical depth (AOD) at 550nm as a metric for aerosol-induced poor visibility. The simulated baseline winter mean AOD around Beijing area is shown in Fig.9a, c. To account for model differences in historical AOD, we used the ratio of AOD at 550nm (hereafter AOD_ratio) relative to a baseline winter mean to represent the air-pollution severity. When AOD_ratio is greater than 1.0, the air-pollution intensity is higher than baseline climate mean. HadGEM3-GC2 and GFDL-CM3 both simulate elevated AOD around Beijing when circulation conditions are favorable ($HWI \geq 1$) (Fig.9 b, d): 1.5 and 1.3 times of the baseline climate mean in HadGEM3-GC2 and GFDL-CM3 respectively. Aerosol and precursor emission increases under CLE (Fig. S1) result in a significant increase in climate winter mean AOD around Beijing in HadGEM3-GC2 (1.1 times) but no significant change in GFDL-CM3, and climate mean AOD in MTR decreases to 0.84 and 0.90 of the baseline climate mean around Beijing in HadGEM3-GC2 and GFDL-CM3, respectively, due to aerosol emissions reduction (Fig.S9).

To check whether poor air quality events still occur even with reduced future aerosol emissions, we show the projected AOD_ratio with $HWI \geq 1$ in Fig.10. In CLE, when $HWI \geq 1$ AOD_ratio is elevated compared to the baseline climatology, to 1.5 times of the baseline winter mean in HadGEM3-GC2 and 1.1 times that in GFDL-CM3 (Fig.10 a, c). It is consistent with the increase in aerosol loadings and climate mean AOD in

Deleted: 4

Deleted: (reaching 1.2 times

Deleted: and

Deleted: 1.05 times

Deleted:),

Deleted: while

Deleted: 93

Deleted: the two models

Deleted: 6

486 CLE (Fig.S2a and Fig.S9a-b). However, in MTFR, when $HWI \geq 1$, AOD is ~~slightly~~
 487 higher (~~AOD_ratio is around 1.1~~), ~~or comparable with that of~~ the baseline climatology.
 488 albeit with a decrease in climate mean AOD in MTFR (Fig.10 b,d). So, even with the
 489 aggressive aerosol reductions in MTFR, periods of poor visibility still occur in
 490 conjunction with atmospheric circulation patterns associated with haze in the current
 491 climate.

492 We calculated the PDF distributions of AOD_ratio surrounding the Beijing region (box
 493 region in Fig.2) in the months with $HWI \geq 1$ in His, CLE and MTFR (Fig.11). In His,
 494 the area-averaged AOD_ratio around the Beijing region when $HWI \geq 1$ is elevated to
 495 ~~1.40~~, (~~1.24~~) times of the baseline climate mean in HadGEM-GC2 (GFDL-CM3).
 496 (Fig11.a-b). The change in AOD_ratio with $HWI \geq 1$ under CLE relative to His is
 497 different between the two models. It increases to ~~1.45~~ in HadGEM3-GC2 but decreases
 498 to ~~1.06~~ in GFDL-GC3. As expected, the AOD_ratio with $HWI \geq 1$ in MTFR reduces in
 499 both models due to the dramatic reduction in anthropogenic aerosols. Thus, the mean
 500 air-pollution intensity with the favorable circulation conditions for haze under MTFR
 501 will be greatly relieved. ~~This reduction in GFDL-CM3 under CLE relative to His may~~
 502 be a reflection of the model's bias. In JRA-55 when $HWI \geq 1$ there are southerly
 503 anomalies over southern China. However, in the baseline in GFDL-CM3 there is an
 504 anomalous cyclonic circulation, which may act to reduce pollutant accumulation in
 505 Beijing (Fig.S5). As shown in Fig. 6b, d, this anomaly is strengthened in both CLE and
 506 MTFR.

Deleted: also

Deleted: than

Deleted: 34

Deleted: 6

Deleted: 51

Deleted: 13

Deleted: -

514 To check whether extreme air pollution events would still occur, the probability of
 515 AOD_ratio when $HWI \geq 1$ in the three scenarios are examined (Fig.11b, d). In this study,
 516 the mean AOD_ratio across all months when $HWI \geq 1$ in His is regarded as the winter
 517 mean intensity of baseline haze events, i.e., the grey vertical lines in Fig.11a, c. The
 518 probability of haze event intensity exceeding this threshold is about 44% and 39% in
 519 HadGEM3-GC2 and GFDL-CM3, respectively (Fig.11b, d). Under CLE, it increases
 520 to 44% in HadGEM3-GC2 while decreases to 23% in GFDL-CM3, consistent with
 521 Fig.10a, c. In MTFR, lower probability is projected in both models, 18% in HadGEM-
 522 GC2, and 19% in GFDL-CM3. This demonstrates that severe events (i.e., higher
 523 AOD_ratio) would still happen in MTFR albeit with dramatic reduction in
 524 anthropogenic aerosol, even though the mean intensity of haze events themselves will
 525 become less dangerous if aerosol emissions are reduced.

526 5 Summary and discussion

527 During recent decades, with rapid increases in aerosol and precursor emissions in China,
 528 air pollution has become one of the greatest threats to public health. Anthropogenic
 529 aerosol contributes not only to the chemical composition of haze, but also has the
 530 potential to modulate atmospheric circulation changes. Thus, this paper aims to
 531 quantify the incidences of haze events in a future climate and the influence of aerosol
 532 mitigation efforts. In this study, we examined the changes in the frequency of
 533 atmospheric conditions conducive to haze events around Beijing region, and the
 534 changes in aerosol optical depth (AOD) during these circulation conditions through the

Deleted: 2

Deleted: 4

Deleted: 52

Deleted: 8

Deleted: 24

Deleted: 21

541 mid-21st century under two different anthropogenic aerosol scenarios using two climate
542 models, HadGEM3-GC2 and GFDL-CM3. We also investigated the mechanism for the
543 changes in the large-scale atmospheric circulation.

544 We found that future greenhouse gases (GHG) increases and anthropogenic aerosol
545 (AA) increases following a current legislation aerosol scenario (CLE) will increase the
546 frequency of haze-favorable atmospheric circulation conditions surrounding the Beijing
547 region. The frequency of haze weather index (HWI) ≥ 1 derived from monthly data in

548 HadGEM3-GC2 (GFDL-GCM3) increases from ~~~16%~~ (16%) at baseline to ~~~22%~~
549 (~~25%~~) for 2015-2049, under the CLE scenario. By comparing the scenario with a

550 maximum technically feasible aerosol reduction (MTFR), which has the same GHG
551 increases but rapid aerosol reductions, we show that future aerosol reductions may
552 further amplify the increase in the frequency of such circulation patterns. Rapid

553 reductions in AA emissions in MTFR contribute to ~~an~~ extra increase in HWI ≥ 1 in two
554 models.

555 The increase in haze frequency in CLE is mainly due to a weakening of the East Asian
556 winter monsoon, warming of the lower troposphere, and weakening of the East Asian
557 trough, which is likely to be predominantly driven by the GHG increases. Reduced AA
558 forcing in MTFR could further enhance the above circulation anomalies and amplify
559 the impact of greenhouse gases. Because the AA emission reductions in MTFR relative
560 to CLE mainly occur over continental Asia, the Asian landmass receives more
561 shortwave radiation, leading to a warmer surface temperature there. This leads to a

Deleted: 18

Deleted: 28

Deleted: 31

Deleted: 6

Deleted: 50

Deleted: an

Deleted: ~6%

569 weaker Siberian high, and further contributes to the weakening of the East Asian winter
570 monsoon in MTFR.

571 The analysis of haze intensity based on AOD at 550 nm shows that visibility with
572 $HWI \geq 1$ is always lower than the baseline winter mean under both CLE and MTFR.

573 With more reduction in aerosol emissions following the MTFR, the mean intensity of
574 haze events in the haze-favorable atmospheric circulation will become less dangerous
575 compared to that in His and CLE in both models. Meanwhile, the probability of haze
576 event with intensity exceeding the baseline mean also decrease in MTFR,
577 demonstrating that severe haze events would also occur in MTFR.

578 This paper reveals the competing impacts of AA emission reductions on haze-favorable
579 circulation and haze intensity surrounding Beijing. AA reductions cause an increased
580 frequency of atmospheric circulation patterns conducive to haze events, but a reduction

581 in the haze intensity when these circulation patterns do occur. Internal variability may
582 not be fully sampled because of limited number of realizations and models used in this
583 study. In addition, the role of single forcing is not discussed here due to both changes
584 in AA and GHGs in CLE and MTFR experiment. We thus further tested roles of AA
585 forcing in driving the HWI changes during 2015-2050 using “all-but-one-forcing”
586 initial-condition large ensembles (LEs) with CESM1 (Deser et al., 2020; Key et al.,
587 2015, Table S2 and Fig.S10 in Supplementary). The large number of ensemble
588 members enables an estimation on internal variability, and an estimation on the signals
589 of regional response to AA or GHGs forcing from the noise of model’s internal

Moved (insertion) [13]

Deleted: But

Deleted: i

variability. Comparing the winter mean HWI of the baseline, it increases under RCP8.5, and both decrease in AA and increase in GHG contribute to the projected higher HWI and more frequent $\text{HWI} \geq 1.0$ (Fig.S10). The response to decrease in AA is significant, as seen from the medium of changes in the projected winter-mean HWI and frequency of month with $\text{HWI} \geq 1$ falling outside the upper quartile of internal variability (Fig.S10). The signal to noise ratio (SNR), defined as the ratio of changes in MME relative to spread across the changes of ensemble members, is higher than 1.0 (1.44) for HWI change when only AA forcing changes in the future (XGHG), consistent with the results derived from HadGEM3-GC2 and GFDL-CM3. The results from CESM-LEs give additional support for the main findings of this study, highlighting the substantial impacts of aerosol forcing for future changes in the atmospheric conditions favoring haze events. A detail examination on the role of single anthropogenic forcing and on the impact of internal variability is needed in the future.

We ~~revealed~~ that the capability of the models in representing haze-favorable large-scale circulations may impact the simulation of AOD, which introduces further uncertainties in future projection of AOD. Model evaluation on haze-favorable circulation and associated AOD is necessary for future projection. Our results are consistent with previous studies that global warming, and more reduction in aerosol forcing caused extra warming, will make haze-favorable conditions around Beijing area more frequent (Callahan and Markin, 2020). Large uncertainty also exists in the projection of AOD and pollutant associated with haze event. Better representation in aerosol parameters

Formatted: Font:12 pt, Font color: Text 1

Formatted: Font:12 pt, Font color: Text 1

Deleted: In the future, single forcing experiments and large ensemble simulations are useful ways to confirm the relative role of greenhouse gases and anthropogenic aerosol forcing on haze events.

Deleted: found

and processes could provide a more reliable way for haze events projection.

Moved up [13]: But internal variability may not be fully sampled because of limited number of realization and models used in this study. In the future, single forcing experiments and large ensemble simulations are useful ways to confirm the relative role of greenhouse gases and anthropogenic aerosol forcing on haze events.

Code/Data availability: The National Climatic Data Center (NCDC) Global Surface Summary of the Day (GSOD) database can be downloaded from the GSOD website (<https://catalog.data.gov/dataset/global-surface-summary-of-the-day-gsod>). The JRA-55 reanalysis data can be freely downloaded from the rda.ucar.edu website (<https://rda.ucar.edu/datasets/ds628.0/>). Requests for outputs of the His, CLE and MTR experiments, or any questions regarding the data, can be directed to the corresponding author, L Zhang (lixiazhang@mail.iap.ac.cn).

Author contribution: L Zhang designed and wrote the manuscript with support from all authors. LJW and MAB helped design the analysis and supervised the work. NJD and DJP ran the simulations. Shuai Hu analyzed the reanalysis data. Donghuan Li and Liwei Zou contributed to the validation of observational metrics.

Competing interests: The authors declare that they have no conflict of interest.

Acknowledgement: This work was jointly supported by the Ministry of Science and Technology of China under Grant 2018YFA0606501 and the National Natural Science Foundation of China under grant No. 41675076. LJW, MAB and JKPS were supported by the UK-China Research & Innovation Partnership Fund through the Met Office Climate Science for Service Partnership (CSSP) China as part of the Newton Fund. Liwei Zou is supported by National Natural Science Foundation of China under grant No. 41830966.

Reference:

Amann, M., Bertok, I., Borken-Kleefeld, J., Cofala, J., Heyes, C., Hoglund-Isaksson, L., Kiesewetter, G., Klimont, Z., Schöpp, W., Vellinga, N., Winiwarter, W.: Adjusted historic emission data, projections, and optimized emission reduction targets for 2030 – A comparison with COM data 2013. Part A: Results for EU-28. TSAP Report #16A, version 1.1. IIASA, Laxenburg, Austria, 2015.

Deleted: I. Bertok, I., J. Borken-Kleefeld, J., J. Cofala, J., C. Heyes, C., L. Hoglund-Isaksson, L., G. Kiesewetter, G., Z. Klimont, Z., W. Schöpp, W., N. Vellinga, N., W.

... 1

An, Z., Huang, R., Zhang, R., Tie, X., Li, G., Cao, J., Zhou, W., Shi, Z., Han, Y., Gu, Z., Ji, Y.: Severe haze in northern China: A synergy of anthropogenic emissions and atmospheric processes. Proceedings of the National Academy of Sciences of the United States of America, 116 (18), 8657–8666, <https://doi.org/10.1073/pnas.1900125116>, 2019.

Deleted: R. Huang, R., R. Zhang, R., X. Tie, X., G. Li, G., J. Cao, J., W. Zhou, W., Z. Shi, Z., Y. Han, Y., Z. Gu, Z., Y.

... 2

Bellouin, N., Rae, J., Jones, A., Johnson, C., Haywood, J., and Boucher, O.: Aerosol forcing in the Climate Model Intercomparison Project (CMIP5) simulations by HadGEM2-ES and the role of ammonium nitrate, J. Geophys. Res., 116, D20206, doi:10.1029/2011JD016074, 2011.

Deleted: J. Rae, J., A. Jones, A., C. Johnson, C., J. Haywood, J., and O.

... 3

Cai, W., Li, K., Liao, H., Wang, H., Wu, L.: Weather conditions conducive to Beijing severe haze more frequent under climate change, Nat. Clim. Change. 7, 257–62, 2017.

Deleted: W. Cai, K. Li, K., H. Liao, H., H. Wang, H., L.

... 4

Callahan, C. W., and Mankin, J. S.: The influence of internal climate variability on projections of synoptically driven Beijing haze. Geophysical Research Letters, 46, e2020GL088548. <https://doi.org/10.1029/2020GL088548>, 2020.

Callahan, C. W., Schnell, J. L., and Horton, D. E.: Multi-index attribution of extreme winter air quality in Beijing, China. Journal of Geophysical Research: Atmospheres, 124, 4567–4583. <https://doi.org/10.1029/2018JD029738>, 2019.

Chakravarti, Laha, and Roy: Handbook of Methods of Applied Statistics, Volume I, John Wiley and Sons, 392-394, 1967.

Chen, H., Wang, H.: Haze Days in North China and the associated atmospheric circulations based on daily visibility data from 1960 to 2012. J. Geophys. Res. Atmos., 120, 5895–5909, <https://doi.org/10.1002/2015JD023225>, 2015.

Deleted: P.

Moved down [1]: H. J.,

Moved (insertion) [1]

Deleted: J.,

719 Chen, H., Wang, H., Sun, J., Xu, Y., Yin, Z.: Anthropogenic fine particulate matter
720 pollution will be exacerbated in eastern China due to 21st century GHG warming.
721 Atmospheric Chemistry and Physics, 19, 233–243, [https://doi.org/10.5194/acp-](https://doi.org/10.5194/acp-19-233-2019)
722 19-233-2019, 2019.

723 China State Council: Action Plan on Prevention and Control of Air Pollution, China
724 State Council, Beijing, China, [http://www.gov.cn/zwgg/2013-](http://www.gov.cn/zwgg/2013-09/12/content_2486773.htm)
725 09/12/content_2486773.htm (last access: 17 January 2021), 2013.

726 Deser, C., Phillips, A., and Coauthors: Isolating the Evolving Contributions of
727 Anthropogenic Aerosols and Greenhouse Gases: A New CESM1 Large Ensemble
728 Community Resource. *J. Clim.*, 33, 7835–7858, 2020.

729 Ding, Y. and Liu, Y.: Analysis of long-term variations of fog and haze in China in
730 recent 50 years and their relations with atmospheric humidity, *Sci. China Earth*
731 *Sci.*, 57, 36–46, 2014.

732 Donner, L., Wyman, B., Hemler, R., Horowitz, L., Ming, Y., et al.: The dynamical
733 core, physical parameterizations, and basic simulation characteristics of the
734 atmospheric component of the GFDL global coupled model CM3. *Journal of*
735 *Climate*, 24, 3484–3519, DOI: 10.1175/2011JCLI3955.1 2011.

736 Feng, J., Quan, J., Liao, H., Li, Y. and Zhao, X.: An Air Stagnation Index to Qualify
737 Extreme Haze Events in Northern China. *Journal of the Atmospheric Sciences*, 75,
738 3489–3505. doi:10.1175/JAS-D-17-0354.1. 2018.

739 Fyfe, J., Boer, G. and Flato, G.: The Arctic and Antarctic oscillations and their projected
740 changes under global warming. *Journal of Geophysical Research*, 26, 1601–1604,
741 1999.

742 Griffies, S., Winton, M., Donner, L., et al.: The GFDL CM3 Coupled Climate Model:
743 Characteristics of the Ocean and Sea Ice Simulations. *Journal of Climate*, 24(13),
744 3520–3544, 2011.

745 Han, Z., Zhou, B., Xu, Y., Wu, J., and Shi, Y.: Projected changes in haze pollution
746 potential in China: an ensemble of regional climate model simulations.

Deleted: H.

Deleted: J.

Deleted: ,Y.

Deleted: Z.

Deleted: H.

Deleted: J.

Moved down [2]: B. L.

Moved (insertion) [2]

Deleted: L.

Moved down [3]: R. S.

Moved (insertion) [3]

Deleted: J.

Deleted: S.

Deleted: L. W.

Deleted: Y.

Deleted: J.

Deleted: H.

Deleted: Y.

Deleted: X.

Deleted: C.

Deleted: J.

Deleted: M.

Deleted: M.

Deleted: L.

Deleted: B.

Deleted: Y.

Deleted: J.

Deleted: Y.

773 Atmospheric Chemistry and Physics, 17, 10109–10123.
 774 <https://doi.org/10.5194/acp-17-10109-2017>, 2017.

775 He, J., Gong, S., Zhou, C. et al.: Analyses of winter circulation types and their impacts
 776 on haze pollution in Beijing. *Atmospheric Environment*, 192, 94–103, 2018.

777 Horton, D., Harshvardhan and Diffenbaugh, N.: Response of air stagnation frequency
 778 to anthropogenically enhanced radiative forcing. *Environ. Res. Lett.*, 7, 044034,
 779 [doi:10.1088/1748-9326/7/4/044034](https://doi.org/10.1088/1748-9326/7/4/044034). 2012.

780 Horton, D., Skinner, C. B., Singh, D., Diffenbaugh, N.: Occurrence and persistence of
 781 future atmospheric stagnation events. *Nature Climate Change*, 4, 698–703, DOI:
 782 [10.1038/NCLIMATE2272](https://doi.org/10.1038/NCLIMATE2272), 2014.

783 Hori, M.E. and Ueda, H.: Impact of global warming on the East Asian winter monsoon
 784 as revealed by nine coupled atmosphere-ocean GCMs. *Geophysical Research*
 785 *Letters*, 33(3), L03713, 2006.

786 Kay, J. E., and Coauthors: The Community Earth System Model (CESM) large
 787 ensemble project: A community resource for studying climate change in the
 788 presence of internal climate variability. *Bull. Amer. Meteor. Soc.*, 96, 1333–1349,
 789 <https://doi.org/10.1175/BAMS-D-13-00255.1>, 2015.

790 Kobayashi, S., and Coauthors: The JRA-55 reanalysis: general specifications and basic
 791 characteristics. *Journal of the Meteorological Society of Japan*, 93(1), 5–
 792 48, doi:<http://doi.org/10.2151/jmsj.2015-001>, 2015.

793 Jeong, J., and Park, R.: Winter monsoon variability and its impact on aerosol
 794 concentrations in East Asia. *Environmental Pollution*, 221, 285e292, 2017.

795 Lamarque, J., Bond, T., Eyring, V., et al.: Historical (1850–2000) gridded
 796 anthropogenic and biomass burning emissions of reactive gases and aerosols:
 797 Methodology and application, *Atmospheric Chemistry and Physics*, 10,
 798 7017–7039, 2010.

Formatted: Indent: Left: 0 cm, Hanging: 2 ch,
 First line: -2 ch

Deleted: ,

Deleted: acin I

Deleted: Rokjin J.

802 Li, Q., Zhang, R., Wang, Y.: Interannual variation of the wintertime fog-haze days
803 across central and eastern China and its relation with East Asian winter monsoon.
804 International Journal of Climatology. 36, 346e354, 2016.

805 Li, K., Liao, H., Cai, W., & Yang, Y.: Attribution of anthropogenic influence on
806 atmospheric patterns conducive to recent most severe haze over eastern China.
807 Geophysical Research Letters, 45, 2072–2081. [https://doi.org/10.1002/](https://doi.org/10.1002/2017GL076570)
808 2017GL076570, 2018.

809 Liu, C., Zhang, F., Miao, L., Lei, Y. & Yang, Q. Future haze events in Beijing, China:
810 When climate warms by 1.5 and 2.0C. Int. J. Climatol., 40, 3689–3700, 2019a.

811 Liu, Z. et al. A Model Investigation of Aerosol Induced Changes in the East Asian
812 Winter Monsoon. Geophys. Res. Lett., 46, 10186–10195, 2019b.

813 Luo, F., Wilcox, L., Dong, B. et al.: Projected near-term changes of temperature
814 extremes in Europe and China under different aerosol emissions. Environmental
815 Research Letters, 15,034013, 2020.

816 Ming, Y., Ramaswamy, V., Donner, L., and Phillips, V.: A robust parameterization of
817 cloud droplet activation. J. Atmos. Sci., 63, 1348–1356, 2006.

818 Niu, F., Li, Z., Li, C., Lee, K.-H., and Wang, M.: Increase of wintertime fog in China:
819 Potential impacts of weakening of the eastern Asian monsoon circulation and
820 increasing aerosol loading. J. Geophys. Res., 115, D00K20,
821 doi:10.1029/2009JD013484, 2010.

822 Pei, L. and Yan, Z.: Diminishing clear winter skies in Beijing towards a possible future.
823 Environmental Research Letters, 13, 124029, 2018.

824 Pei, L., Yan, Z., Sun, Z., Miao, S., Yao, Y.: Increasing persistent haze in Beijing:
825 potential impacts of weakening East Asian winter monsoons associated with
826 northwestern Pacific sea surface temperature trends. Atmospheric Chemistry and
827 Physics, 18,3173–83, 2018.

828 Pei, L., Yan Z., Chen D., and Miao S.: Climate variability or anthropogenic emissions:
829 which caused Beijing Haze? Environmental Research Letters, 15 034004, 2020.

Deleted: L.

Deleted: B.

Deleted: L. J.

Moved down [4]: V. T. J.

Moved (insertion) [4]

Deleted: V.

Deleted: T. J.

Moved down [5]: Z. Q.

Moved (insertion) [5]

Moved (insertion) [7]

Deleted: . Q.

Deleted: C.

Moved down [6]: K.-H.

Moved (insertion) [6]

Deleted:

Moved down [7]: M. Y.

Deleted: Y.

Moved down [8]: Z. W.,

Moved (insertion) [8]

Deleted: W.,

Deleted: Z.W,

Deleted: Z.

Deleted: S.

Deleted: Y.

Deleted: W.

850 Scannell, C., and Coauthors: The Influence of Remote Aerosol Forcing from
 851 Industrialized Economies on the Future Evolution of East and West African
 852 Rainfall. *Journal of Climate*, 32, 8335–8354, [https://doi.org/10.1175/JCLI-D-18-](https://doi.org/10.1175/JCLI-D-18-0716.1)
 853 0716.1. 2019.

854 Shindell, D., Miller, R., Schmidt, G., Pandolfo, L.: Simulation of recent northern
 855 winter climate trends by greenhouse-gas forcing. *Nature*, 399, 452–455, 1999.

856 Taylor, K., Stouffer B., and Meehl, G.: An overview of CMIP5 and the experiment
 857 design, *Bull. Am. Meteorol. Soc.*, 93, 485–498, 2012.

858 Wang, H., Chen, H., and Liu, J.: Arctic sea ice decline intensified haze pollution in
 859 eastern China, *Atmospheric and Oceanic Science Letters*, 1–9, 2015.

860 Wang, L., Chen, W.: An intensity index for the east Asian winter monsoon. *Journal of*
 861 *Climate*, 27, 2361. <https://dx.doi.org/10.1175/JCLI-D-13-00086.1>, 2014.

862 Wang, Y., Le, T., Chen, G., et al.: Reduced European aerosol emissions suppress winter
 863 extremes over northern Eurasia. *Nature Climate Change*, 10, 225–230, 2020.

864 [Wilcox L J, Liu Z, Samset B H, et al.: Accelerated increases in global and Asian summer](#)
 865 [monsoon precipitation from future aerosol reduction. *Atmospheric Chemistry and*](#)
 866 [Physics, 20\(20\), 11955-11977. <https://doi.org/10.5194/acp-20-11955-2020>, 2020.](#)

867 Williams, K., Harris, C., Bodas-Salcedo, A., et al.: The Met office global coupled model
 868 2.0 (GC2) configuration *Geoscientific Model Development*, 8, 1509–24, 2015.

869 Wu, P., Ding, Y., Liu, Y.: Atmospheric circulation and dynamic mechanism for
 870 persistent haze events in the Beijing–Tianjin–Hebei region. *Advances in*
 871 *Atmospheric Sciences*, 34, 429–40, doi: 10.1007/s00376-016-6158-z. 2017.

872 [Zhang, H., and T. L. Delworth: Robustness of anthropogenically forced decadal](#)
 873 [precipitation changes projected for the 21st century. *Nat Commun*, 9, 1150, doi:](#)
 874 [10.1038/s41467-018-03611-3, 2018.](#)

875 Zhang, R., Li, Q., Zhang, R.: Meteorological conditions for the persistent severe fog
 876 and haze event over eastern China in January. *Science China Earth Sciences*, 57,
 877 26–35. <https://doi.org/10.1007/s11430-013-4774-3>, 2014.

Moved down [9]: R. L.
Deleted: T.
Moved (insertion) [9]
Deleted: L. G. A.
Deleted: L.
Deleted: E.
Deleted: J.
Deleted: A.
Deleted: J.,
Moved down [10]: H. P.
Moved (insertion) [10]
Deleted: P.
Moved down [11]: J. P.
Moved (insertion) [11]
Deleted: P.
Deleted: T.
Deleted: G.
Deleted: D.
Moved down [12]: C. M.
Moved (insertion) [12]
Deleted: . M.
Deleted: A.
Deleted: Y.
Deleted: Y.
Deleted: H.
Deleted: N.

900 Zhang, Y., Yin, Z., Wang H.: Roles of climate variability on the rapid increases of early
901 winter haze pollution in North China after 2010. Atmos. Chem. Phys., 20, 12211–
902 12221, 2020.

903 Zheng, B., Tong, D., Li, M., et al: Trends in China's anthropogenic emissions since
904 2010 as the consequence of clean air actions. Atmospheric Chemistry and Physics,
905 18, 14095–111, 2018.

906
907

Deleted: J.

Deleted:

Deleted: C.

Deleted: J.

Deleted: D.

Deleted: M.

Deleted: Page Break

-

Formatted: Left, Indent: Left: 0 cm, First line:
0 cm, Space Before: 0 pt, After: 0 pt, Line
spacing: single, Widow/Orphan control

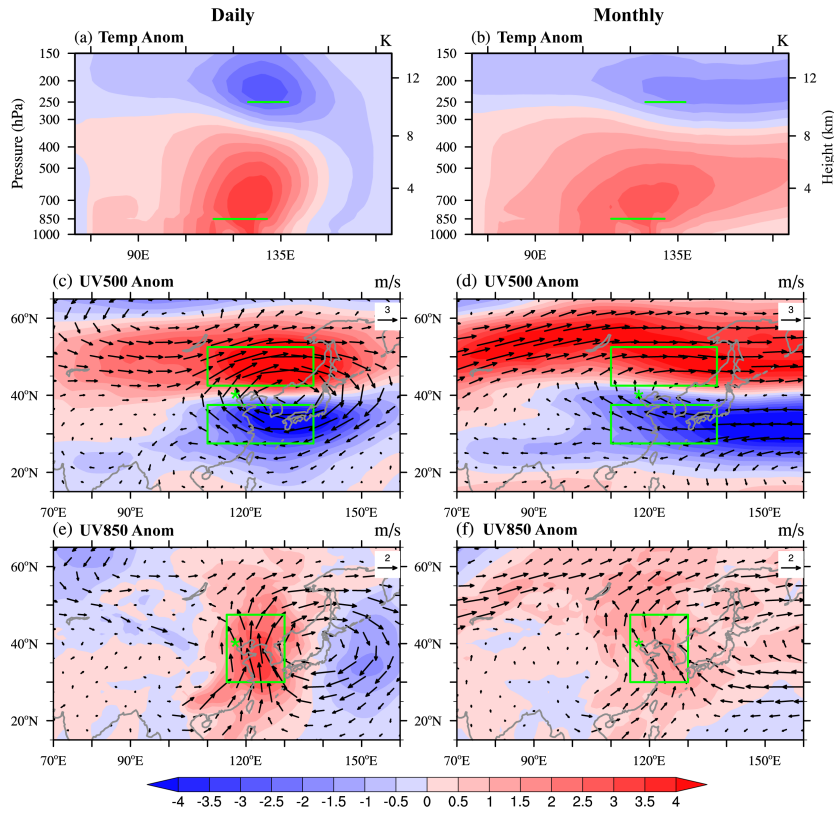


Fig. 1 Composite circulation anomalies from JRA-55 with HWI-daily>0 (left) and HWI-month \geq 1 (right) for 1958-2013. (a)-(b) temperature (K) along 40°N, (c)-(d) 500hPa winds (vector, m s^{-1}) and its zonal component (shading, m s^{-1}). (e)-(f) 850hPa winds (vector, m s^{-1}) and its meridional component (shading, m s^{-1}). The green boxes/lines indicate the regions used to calculate the three components of HWI.

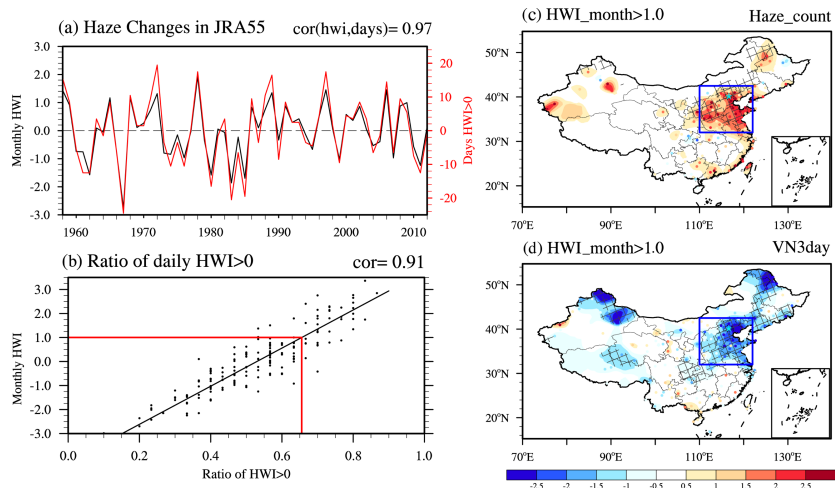


Fig.2 Changes in winter HWI from 1958 to 2013 in JRA-55 reanalysis relative to 1958-2013 winter mean. (a) DJF mean monthly-based HWI (HWI-month, black line) and the anomalous days with daily based HWI>0 (HWI-daily, red line, unit: day), (b) scatter plot of HWI-month of December, January and February (y-axis) and the ratio of days with HWI-daily>0 (x-axis) in each winter month. HWI-month and HWI-daily are the HWI calculated from monthly data and daily data, respectively. (c)-(d) are the anomalies of haze occurrence and the VN3day when $\text{HWI} \geq 1$, where VN3day is the minimum 3-day consecutive visibility. Cross area in (c)-(d) is statistically significant at the 10% level using a Student's t-test.

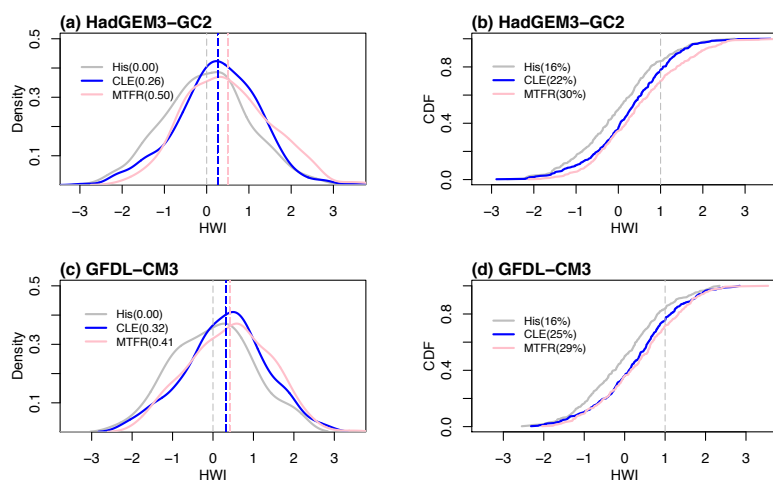
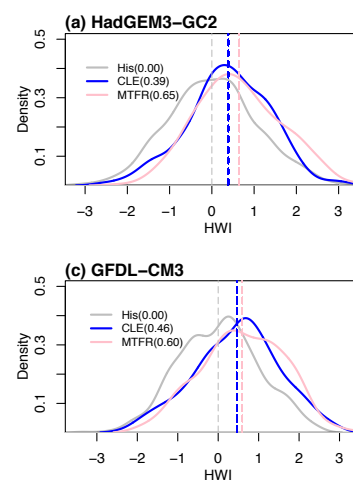


Fig. 3 (a) Probability density function (PDF) via a non-parametric density estimation, Kernel density estimation, and (b) cumulative distribution function (CDF) distributions of HWI in winters of His (1984-2013, grey), CLE (2015-2049, blue) and MTFR (2015-2049, pink) simulated by HadGEM3-GC2. (c)-(d) are results for GFDL-CM3. The numbers in (a) and (c) are the climate mean of HWI, and in (b) and (d) are the frequency of month with $HWI \geq 1$, respectively.



Deleted:

Formatted: Font: (Default) Times New Roman, Font color: Text 1

Deleted: 0

Deleted: 04

Deleted: 6

Deleted: 50

Deleted: 6

Deleted: 50

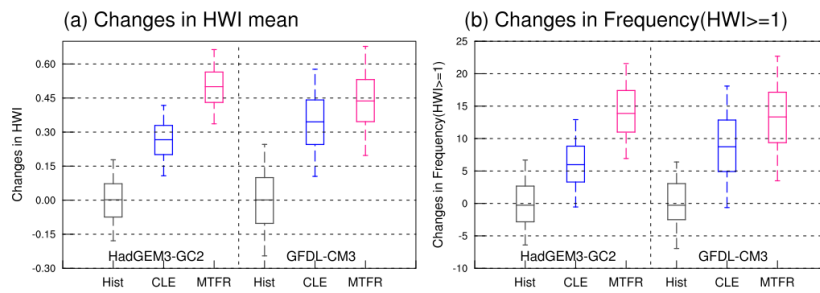
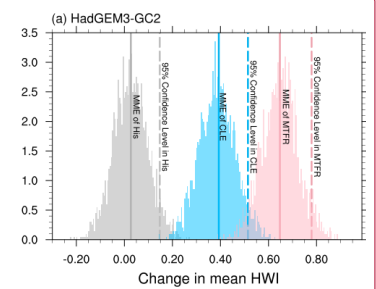
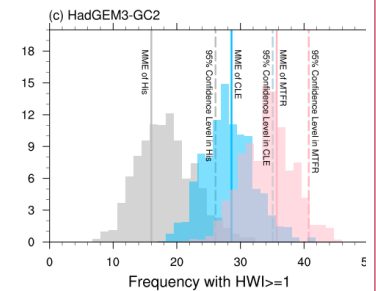


Fig. 4 Box plots for the 5000 bootstrapped samples of (a) changes in winter mean HWI, and (b) frequency of month with $HWI \geq 1$ in HadGEM3-GC2 and GFDL-CM3. The grey, blue and pink boxes are results estimated from Hist, CLE and MTFR respectively. Boxes show the interquartile ranges of the 5000 bootstrapped samples, and black lines show the median. End points are the 5th and 95th percentiles. Significant difference is seen when the median from one experiment falls outside the interquartile range of another.



Deleted:

Formatted: Font: (Default) Times New Roman, Bold, Font color: Text 1



Deleted:

Formatted: Font: (Default) Times New Roman, Bold, Font color: Text 1

Deleted: Histogram

Deleted: 2

Deleted: c

Deleted: , and (b), (d) similarly for

Deleted: shadings

Deleted: the

Deleted:

Deleted: Solid (dashed) grey, blue and pink lines are the results of multi-member mean (95% confidence level) in Hist, CLE and MTFR, respectively.

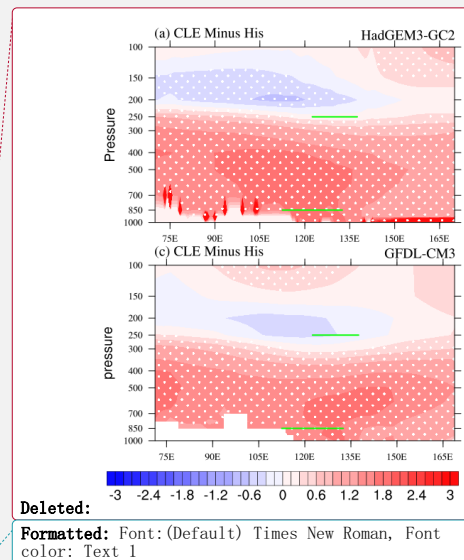
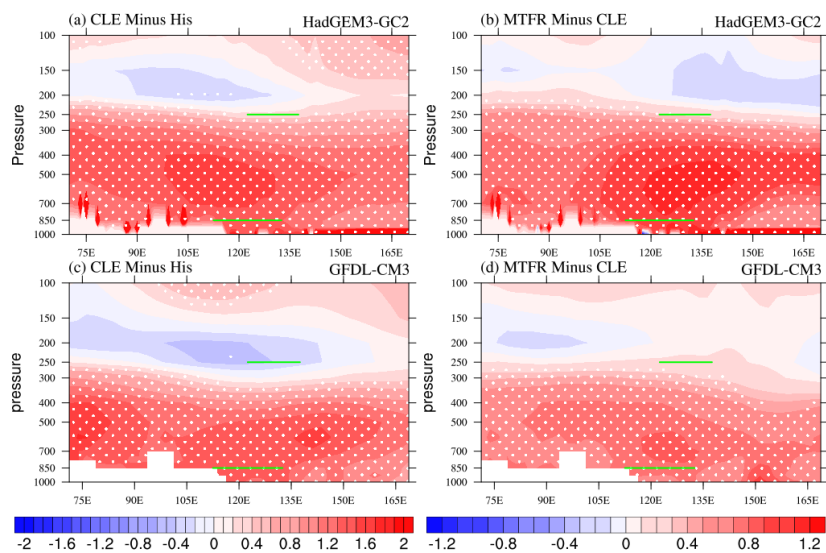


Fig.5 The difference in winter mean temperature (K) along 40°N (left) between CLE (2015-2049) and His (1984-2013), and (right) between MTFR (2015-2049) and CLE (2015-2049). The dotted areas are statistically significant at the 10% level using a Student's t-test. The green lines indicate the level and longitude used in the calculation of ΔT .

Deleted: 6

Deleted: 50

Deleted: 0

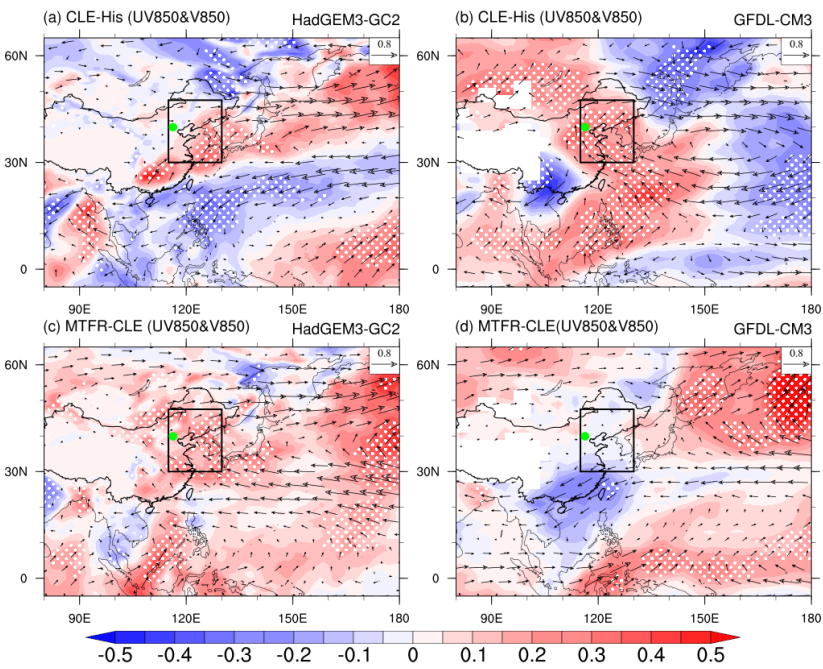
Deleted: 04

Deleted: 6

Deleted: 50

Deleted: 6

Deleted: 50



995

996

997

998

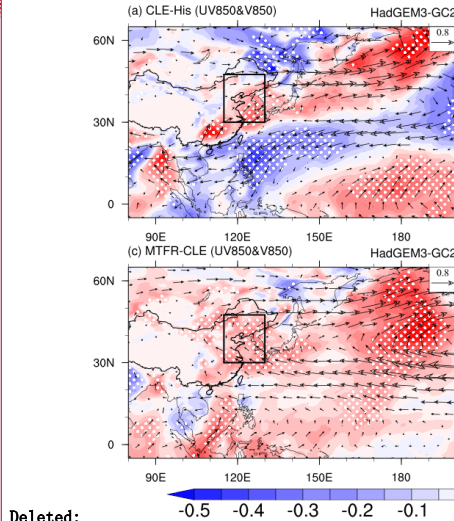
999

1000

1001

1002

Fig.6 Spatial distribution for the difference in winter mean 850 hPa winds (vector, m s^{-1}) and 850hPa meridional component (shading, m s^{-1}) (left) between CLE (2015-2049) and His (1984-2013), and (right) between MTFR (2015-2049) and CLE (2015-2049). The dotted areas denote the 850hPa meridional winds statistically significant at the 10% level using a Student's t-test. The black box indicates the region used in the calculation of V850.



Deleted: -0.5 -0.4 -0.3 -0.2 -0.1
Formatted: Font:(Default) Times New Roman, Font color: Text 1

Deleted: 6
Deleted: 50
Deleted: 0
Deleted: 04
Deleted: 6
Deleted: 50
Deleted: 6
Deleted: 50

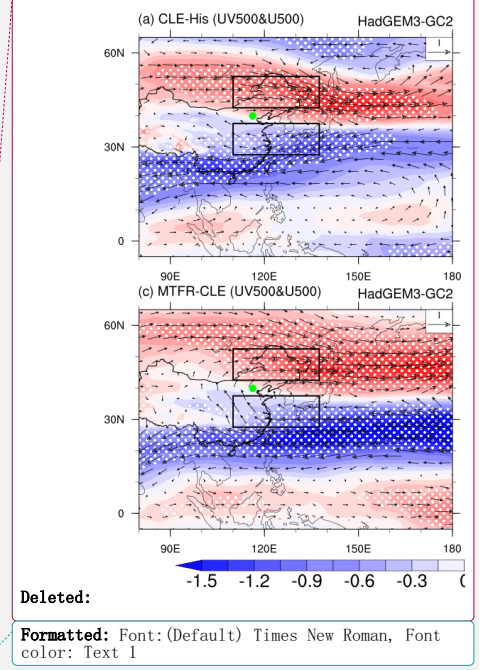
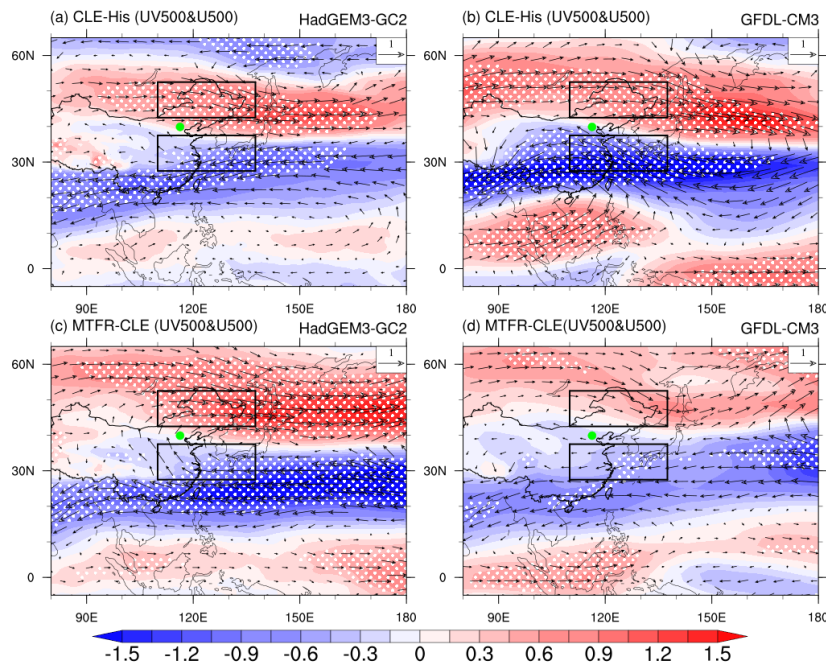


Fig.7 Same as Fig.6, but for the difference in 500hPa winds (vector, m s^{-1}) and 500hPa zonal component (shading, m s^{-1}). The black boxes indicate the regions used in the calculation of U500.

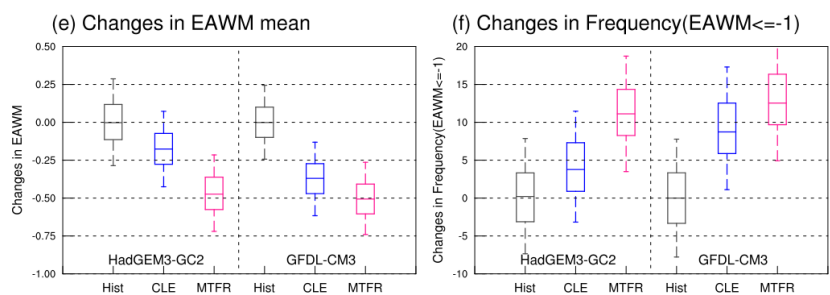
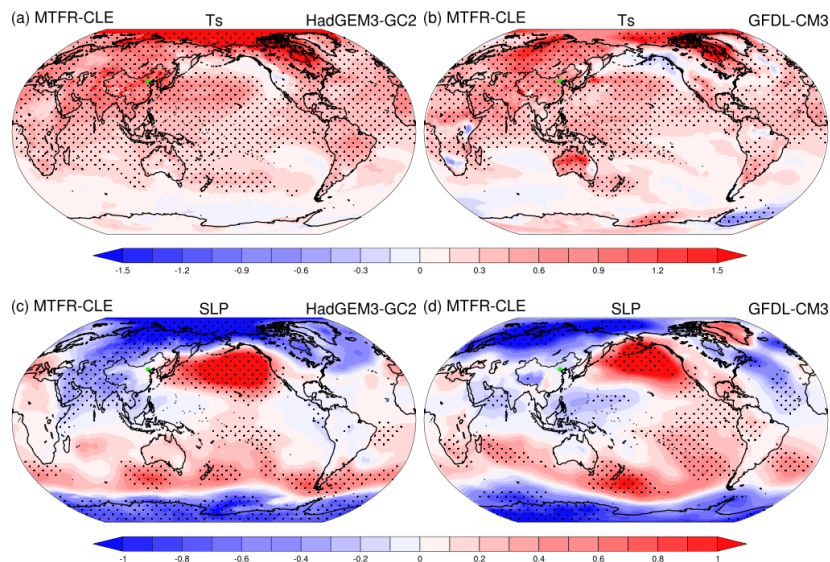
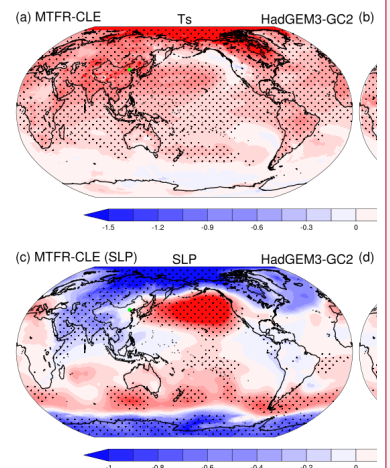
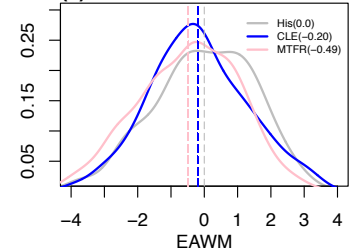


Fig.8 The difference of the climate mean surface temperature (left, K) and sea level pressure (right, hPa) between MTFR and CLE simulated by (a)-(b) HadGEM3-GC2 and (c)-(d) GFDL-CM3. The dotted areas in (a)-(d) are statistically significant at the 10% level using a Student's t-test. (e)-(f) are same as Fig.4, but for changes in the climate mean EAWM and the frequency of $EAWM \leq -1$ in His (1984-2013, grey), CLE (2015-2049, blue) and MTFR (2015-2049, pink).



(e) HadGEM3-GC2



Deleted:

Formatted: Font: (Default) Times New Roman, Font color: Text 1

Deleted: PDF via Kernel density estimation of

Deleted: 0

Deleted: 04

Deleted: 6

Deleted: 50

Deleted: 6

Deleted: 50

Deleted:) simulated by (e) HadGEM3-GC2, and (f) GFDL-CM3

Deleted: The numbers in (e)-(f) are the climate mean of EAWM.

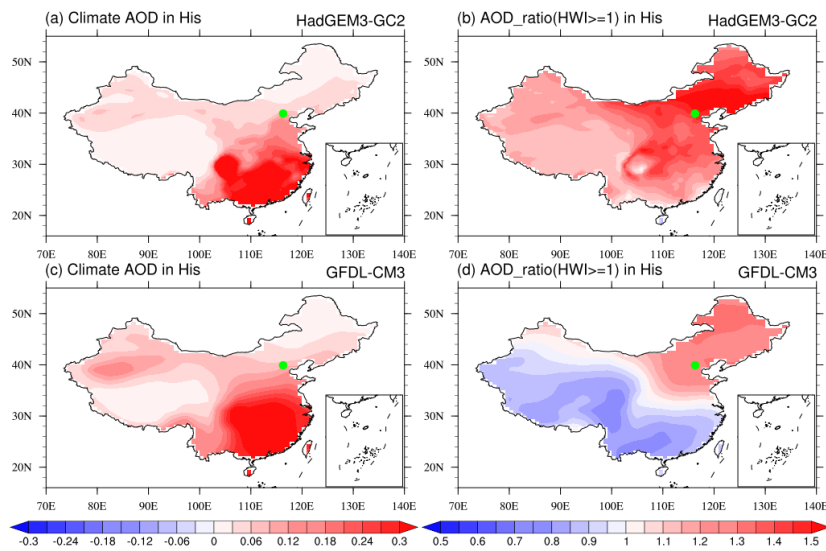
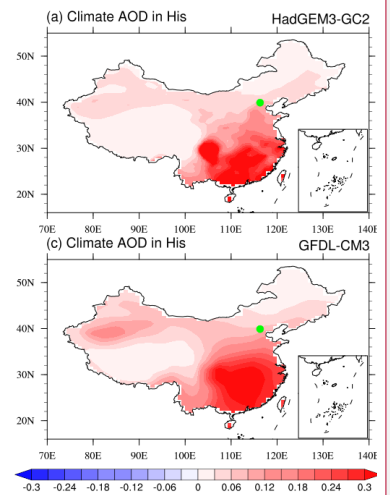


Fig.9 Winter mean (left) AOD at 550 nm in (a) HadGEM3-GC2 and (c) GFDL-CM3 averaged over 1984-2013. Right is same as left, but for the mean AOD ratio in the winter months with $HWI \geq 1$ (hereafter AOD_ratio($HWI \geq 1$)) in His. Blue and red shadings in (b) and (d) are decreased and elevated AOD relative to the climate winter mean of His, respectively.



Deleted:

Formatted: Font:(Default) Times New Roman, Font color: Text 1

Deleted: 0

Deleted: 04

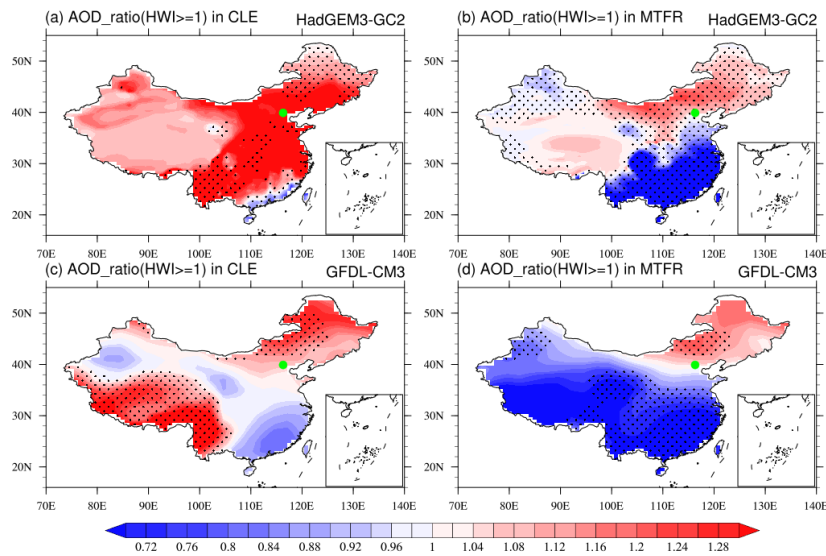
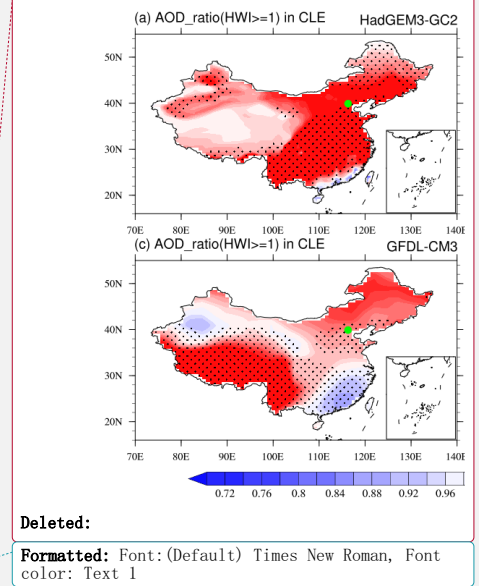


Fig 10. Same as Fig.9b and d, but for the results projected in CLE and MTFR. The dotted areas are statistically significant at the 10% level using a Student's t-test.



Deleted:

Formatted: Font:(Default) Times New Roman, Font color: Text 1

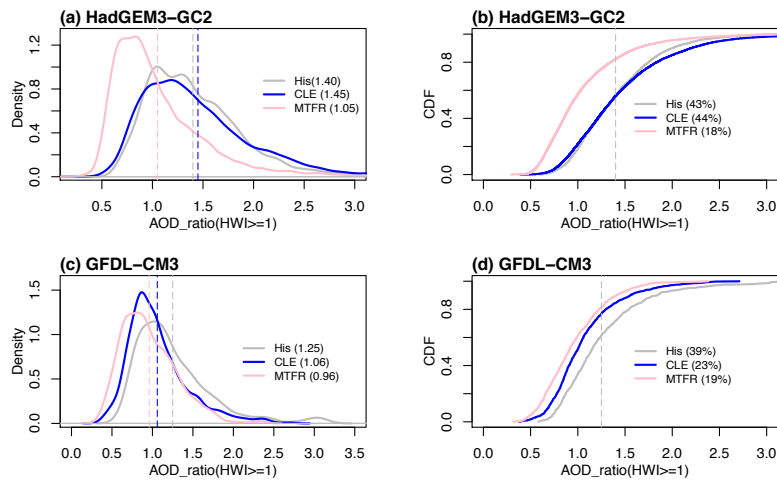
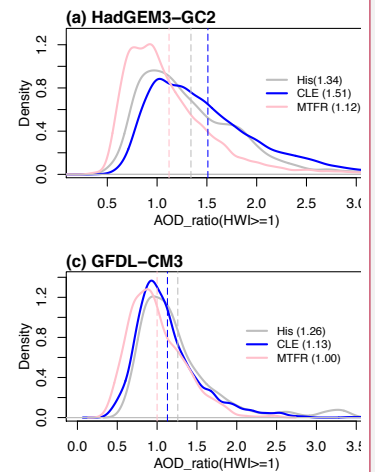


Fig.11 (a) PDF and (b) CDF distributions of AOD_ratio(HWI \geq 1) over North China (33-45°N, 105-122°E, box in Fig.2) in HadGEM3-GC2. (c)-(d) are the results from GFDL-CM3. The grey, blue and pink vertical lines and numbers in (a) and (c) are the winter mean AOD_ratio(HWI \geq 1) of His, CLE and MTFR, respectively. The numbers in (b) and (d) are the cumulative probability of AOD_ratio(HWI \geq 1) higher than the winter mean AOD_ratio(HWI \geq 1) of His.

Formatted: Font: (Default) Times New Roman, Font color: Text 1



Deleted:

Page 26: [1] Deleted	Microsoft Office 用户	4/4/21 1:16:00 PM
----------------------	---------------------	-------------------

I.

Page 26: [1] Deleted	Microsoft Office 用户	4/4/21 1:16:00 PM
----------------------	---------------------	-------------------

I.

Page 26: [1] Deleted	Microsoft Office 用户	4/4/21 1:16:00 PM
----------------------	---------------------	-------------------

I.

Page 26: [1] Deleted	Microsoft Office 用户	4/4/21 1:16:00 PM
----------------------	---------------------	-------------------

I.

Page 26: [1] Deleted	Microsoft Office 用户	4/4/21 1:16:00 PM
----------------------	---------------------	-------------------

I.

Page 26: [1] Deleted	Microsoft Office 用户	4/4/21 1:16:00 PM
----------------------	---------------------	-------------------

I.

Page 26: [1] Deleted	Microsoft Office 用户	4/4/21 1:16:00 PM
----------------------	---------------------	-------------------

I.

Page 26: [1] Deleted	Microsoft Office 用户	4/4/21 1:16:00 PM
----------------------	---------------------	-------------------

I.

Page 26: [1] Deleted	Microsoft Office 用户	4/4/21 1:16:00 PM
----------------------	---------------------	-------------------

I.

Page 26: [1] Deleted	Microsoft Office 用户	4/4/21 1:16:00 PM
----------------------	---------------------	-------------------

I.

Page 26: [2] Deleted	Microsoft Office 用户	4/4/21 1:17:00 PM
----------------------	---------------------	-------------------

R.

Page 26: [2] Deleted	Microsoft Office 用户	4/4/21 1:17:00 PM
----------------------	---------------------	-------------------

R.

Page 26: [2] Deleted	Microsoft Office 用户	4/4/21 1:17:00 PM
----------------------	---------------------	-------------------

R.

Page 26: [2] Deleted	Microsoft Office 用户	4/4/21 1:17:00 PM
----------------------	---------------------	-------------------

R.

Page 26: [2] Deleted	Microsoft Office 用户	4/4/21 1:17:00 PM
----------------------	---------------------	-------------------

R.

Page 26: [2] Deleted	Microsoft Office 用户	4/4/21 1:17:00 PM
----------------------	---------------------	-------------------

R.

Page 26: [2] Deleted	Microsoft Office 用户	4/4/21 1:17:00 PM
----------------------	---------------------	-------------------

R.

Page 26: [2] Deleted	Microsoft Office 用户	4/4/21 1:17:00 PM
----------------------	---------------------	-------------------

R.

Page 26: [2] Deleted	Microsoft Office 用户	4/4/21 1:17:00 PM
----------------------	---------------------	-------------------

R.

Page 26: [2] Deleted	Microsoft Office 用户	4/4/21 1:17:00 PM
----------------------	---------------------	-------------------

R.

Page 26: [3] Deleted	Microsoft Office 用户	4/4/21 1:18:00 PM
----------------------	---------------------	-------------------

J.

Page 26: [3] Deleted	Microsoft Office 用户	4/4/21 1:18:00 PM
----------------------	---------------------	-------------------

J.

Page 26: [3] Deleted	Microsoft Office 用户	4/4/21 1:18:00 PM
----------------------	---------------------	-------------------

J.

Page 26: [3] Deleted	Microsoft Office 用户	4/4/21 1:18:00 PM
----------------------	---------------------	-------------------

J.

Page 26: [3] Deleted	Microsoft Office 用户	4/4/21 1:18:00 PM
----------------------	---------------------	-------------------

J.

Page 26: [4] Deleted	Microsoft Office 用户	4/4/21 1:19:00 PM
----------------------	---------------------	-------------------

J

Page 26: [4] Deleted	Microsoft Office 用户	4/4/21 1:19:00 PM
----------------------	---------------------	-------------------

J

Page 26: [4] Deleted	Microsoft Office 用户	4/4/21 1:19:00 PM
----------------------	---------------------	-------------------

J

Page 26: [4] Deleted	Microsoft Office 用户	4/4/21 1:19:00 PM
----------------------	---------------------	-------------------

J

Page 26: [4] Deleted	Microsoft Office 用户	4/4/21 1:19:00 PM
----------------------	---------------------	-------------------

J